SANDIA REPORT
SAND2018-10507
Unlimited Release
Printed September 2018

LDRD 191204: Optimization of Sputtered Aluminum Nitride for the Seeding of Metal Organic Chemical Vapor Deposition Gallium Nitride Films

Katherine E. Knisely[1]

[1]Sandia National Laboratories, Albuquerque, NM

Prepared by
Sandia National Laboratories
Albuquerque, New Mexico 87185 and Livermore, California 94550

Sandia National Laboratories is a multimission laboratory managed and operated by National Technology and Engineering Solutions of Sandia, LLC, a wholly owned subsidiary of Honeywell International, Inc., for the U.S. Department of Energy's National Nuclear Security Administration under contract DE-NA0003525.


Sandia National Laboratories

Issued by Sandia National Laboratories, operated for the United States Department of Energy by National Technology and Engineering Solutions of Sandia, LLC.

Available to DOE and DOE contractors from

U.S. Department of Energy
Office of Scientific and Technical Information
P.O. Box 62
Oak Ridge, TN 37831

Telephone: (865) 576-8401
Facsimile: (865) 576-5728
E-Mail: reports@osti.gov
Online ordering: http://www.osti.gov/scitech

Available to the public from

U.S. Department of Commerce
National Technical Information Service
5301 Shawnee Rd
Alexandria, VA 22312

Telephone: (800) 553-6847
Facsimile: (703) 605-6900
E-Mail: orders@ntis.gov
Online order: https://classic.ntis.gov/help/order-methods/

SAND201X-XXXX
Printed September 2018
Unlimited Release

LDRD 191204: Optimization of Sputtered Aluminum Nitride for the Seeding of Metal Organic Chemical Vapor Deposition Gallium Nitride Films

Katherine E. Knisely – MESAFab, 5247[1]
[1]K. Knisely is now with Org. 2631
Sandia National Laboratories
P. O. Box 5800
Albuquerque, New Mexico 87185-MS0646

Abstract

GaN-on-Si combines the wide bandgap advantages of GaN with the cost and scaling advantages of Si. Sputtered AlN is an attractive nucleation layer material because it reduces Al diffusion into the Si and eliminates a time-intensive preconditioning step in the GaN growth process, but is limited by the poor film quality of PVD AlN films deposited on Si substrates. Sputtering also offers a large degree of control over AlN film properties, including control of the intrinsic stress using substrate biasing. Doping the AlN films with Sc improves the lattice match to AlGaN and GaN films by expanding the a-axis and c-axis lattice parameters. AlN and $Al_{0.88}Sc_{0.12}N$ films have been grown on silicon, metal, and sapphire substrates and characterized for properties such as stress, grain size, roughness, and film orientation for use as nucleation layers for MOCVD GaN growth.

ACKNOWLEDGMENTS

This work was funded by the Sandia Laboratory Directed Research and Development program under LDRD project 191204.

Thin film analysis was performed by Mark Rodriquez, Paul Kotula, John Mudrick, Michael Busse, Bram Hunt, and Brian Troelsen. Film development was performed at the Sandia MESA SiFab facility, with valuable tool and process contributions from the MESA operations team.

GaN depositions were performed by Dan Koleske, and AlGaN depostions were done by Andrew Allermann.

Rafael Gonzales, Ann Petersen, Erica Douglas, and Ben Griffin provided valuable project management guidance and support.

TABLE OF CONTENTS

FIGURES

TABLES

NOMENCLATURE

Abbreviation	Definition
Abbreviation	Definition
AFM	Atomic force microscopy
Al	Aluminum
AlCu	Aluminum copper (0.5% copper)
AlN	Aluminum nitride
CMOS	Complementary metal oxide silicon
DC	Direct current
DOE	Department of Energy
FWHM	Full width half maximum
IMP	Ionized metal plasma
k	Extinction coefficient
MEMS	Microelectromechanical systems
Mo	Molybdenum
MOCVD	Metalorganic chemical vapor deposition
n	Refractive index
nm	Nanometers
NL	Nucleation layer
Pt	Platinum
PVD	Physical vapor deposition
RF	Radio frequency
Rq	Root mean square roughness
SEM	Scanning electron microscopy
Sc	Scandium
Si	Silicon
SNL	Sandia National Laboratories
TEM	Transmission electron microscopy
Ta	Tantalum
Ti	Titanium
TiN	Titanium nitride
XRD	X-ray diffraction
µm	Micrometer, or micron

1. INTRODUCTION

Integration of metalorganic chemical vapor deposition (MOCVD) III-V films with CMOS back end of line (BEOL) technology allows for the development LEDs and power electronics with smaller footprints and improved electrical routing and signal integrity. This is best achieved using Si substrates, as sapphire substrates are expensive and are often incompatible with CMOS BEOL tools. However, III-V growth on Si wafers is sparsely covered in literature, due to the challenges of achieving buffer layer that can properly orient the III-V film on lattice mismatched substrates such as Si and due to proprietary controls over developments in this field. Sputtered AlN is an attractive buffer layer material, as it is a scalable, CMOS compatible, and has been demonstrated to seed high quality MOCVD GaN films on sapphire substrates. This project's goal was to leverage the existing exceptional III-V and sputtered AlN capabilities at MESAFab to explore and characterize the material science governing MOCVD film growth on Si substrates using sputtered AlN as a seed layer, ultimately benefitting applications such as LEDs, MEMS, and power electronics. The project focus focused on characterizing how factors such as AlN grain size, stress, thickness, and the underlying substrate material properties affect the MOCVD films' growth behavior.

1.1. Background

The objective of this project was to utilize the unique combination of CMOS, sputtered AlN, and MOCVD deposition capabilities available in MESAFab to address the question of what sputtered AlN properties, such as grain size, grain orientation, film stress, and film thickness, are necessary for the nucleation and growth of high quality MOCVD III-V materials on substrates processed using CMOS back end of the line (BEOL) technology. Sputtered AlN has the unique ability to facilitate III-V growth on Si wafers, as sputtered AlN retains a high level of lattice match for MOCVD GaN layer nucleation without requiring a lattice-matched underlying substrate. This project focused on characterizing what sputtered AlN film conditions are required to optimize the growth of MOCVD GaN films on Si wafers, with and without underlying metallization.

1.2. Project Goals

The primary objective of this research was to characterize how the deposition and growth of sputtered AlN on Si wafers, with and without refractory metal layers, affects the nucleation and growth of MOCVD GaN and MOCVD AlN films. Both substrate preparation and AlN deposition parameters affect the quality and film properties of sputtered AlN films. The stress, thickness, bombardment energetics, grain size, and stoichiometry of the sputtered AlN can also be varied through control of the deposition temperature, gas flows, RF bias power, and target power. This project focused on how characterizing these factors with the goal of improving the film conditions for subsequent MOCVD film growth. This included characterizing AlN and $Al_{0.88}Sc_{0.12}N$ films on Si and oxide, including analysis of film properties such as grain size, roughness, residual stress and intrinsic stress gradients, and film orientation. Additionally, AlN films were deposited and characterized on TiN and Ta, which are

CMOS-compatible substrates which have not been previously well characterized. Additionally, doping AlN films with Sc to form $Al_{0.88}Sc_{0.12}N$ increases the a-axis and c-axis lattice parameters, improving the lattice match to GaN or AlGaN films, so this project also grew to include characterization of $Al_{0.88}Sc_{0.12}N$ film growth on Si and sapphire substrates.

1.3. Significant Accomplishments

The significant accomplishments of this project are as follows:

1. A model for predicting the AlN intrinsic film stress was developed. A technique for controlling the AlN intrinsic stress using multiple depositions was experimentally validated using AlN released cantilevers. Using this model, the residual and local stress and strain states of AlN films can be tailored to minimize cracking in subsequently deposited GaN films.

2. AlN films were grown on TiN, AlCu, oxide, and Ta, in order to evaluate whether a metal interlayer deposited between the AlN and the Si substrate would improve AlN orientation. AlN films grown on AlCu had excellent properties, but AlCu is not compatible with the high temperatures used in MOCVD GaN growth. AlN films grown on TiN were of poor quality, and AlN films grown on oxide and Ta showed similar film orientation to those grown on Si. AlN grown on Ta may be of further interest for high temperature piezoelectric applications.

3. GaN films were grown on sputtered AlN films. These films showed some c-axis orientation, but the GaN orientation was limited by the quality of the orientation of the AlN films.

4. AlScN (12% Sc) films grown on Si(111) and Si(100) were characterized for film properties such as texture, roughness, grain size, and stress for a variety of $Al_{0.88}Sc_{0.12}N$ film thicknesses. $Al_{0.88}Sc_{0.12}N$ film orientation improves and the films coarsen as the film thickens. Doping AlN with Sc was found to expand the a-axis and c-axis lattice parameters, resulting in an improved lattice match to GaN.

5. A process was developed to deposit $Al_{0.88}Sc_{0.12}N$ films on sapphire substrates to evaluate whether epitaxial growth of $Al_{0.88}Sc_{0.12}N$ on sapphire improved the $Al_{0.88}Sc_{0.12}N$ orientation. The films showed some c-axis orientation, but large secondary grain growths were also observed. A high temperature anneal may improve the film texture, and further work is being done to evaluate $Al_{0.88}Sc_{0.12}N$ for use as a nucleation layer for AlGaN growth on sapphire.

2. ALN OPTIMIZATION

2.1. Stress Characterization and Control

Sputtered AlN films deposited at low temperatures (350 °C) typically contain large intrinsic stress gradients. The film initially nucleates compressively, but as the films coarsen the grains “zip” together, forming a compressive to tensile film stress gradient as the film thickens, where thicker AlN films have more tensile residual stresses than thinner AlN films [1,2]. Tailoring the strain state of NLs can be used to reduce

cracking defects of subsequently deposited GaN films [3], so it is important to characterize and control the stress/strain states of the AlN NL films. The AlN stress gradient is characterized and controlled using RF substrate bias in Knisely, et al. 2018 [4].

2.2. Effect of Vacuum Quality on AlN Orientation

When the vacuum conditions are insufficient during AlN deposition, secondary grains, also commonly called "inclusions," can nucleate and grow in the films [5]. A planar SEM image of a well oriented AlN film is shown in Figure 1a, and planar and cross-section SEM images of an AlN film with inclusions is shown in Figure 1b. The inclusions have been identified as secondary grain growths in the AlN 10·1, 10·2, and 10·3 direction, and have been shown to reduce piezoelectric coupling [6,7]. Additionally, a higher density of inclusions results in decreased c-axis film orientation; the AlN(002) rocking curve improves as the inclusion density decreases, as shown in Figure 2. In order to achieve AlN films with sufficiently good orientation for use as GaN NLs it is critical to obtain the lowest vacuum possible prior to deposition.

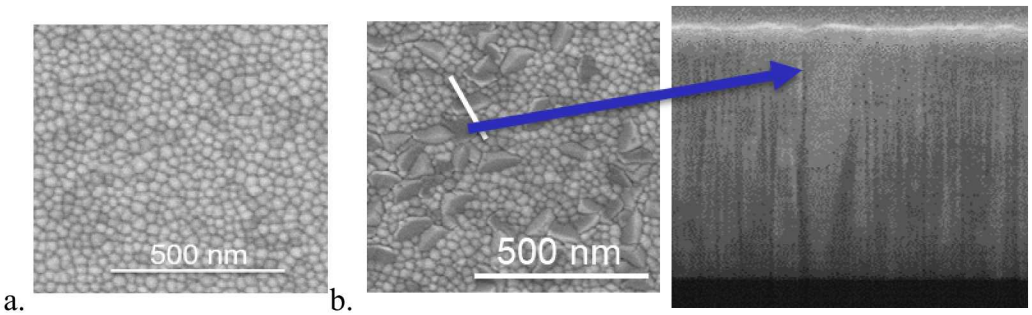

a. b.

Figure 1. A planar SEM image of a well oriented AlN film (a), and a planar (left, b) and cross-section (right, b) image of an AlN film containing AlN(101) inclusions

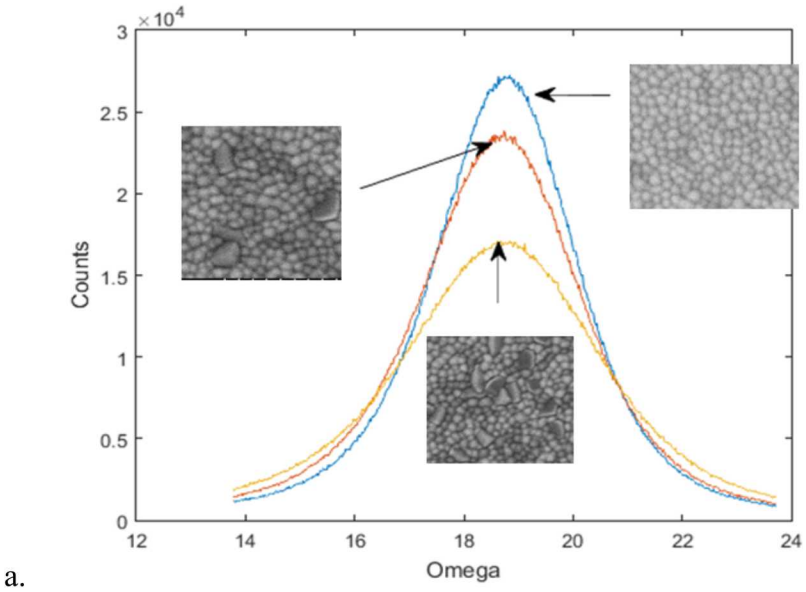

a.

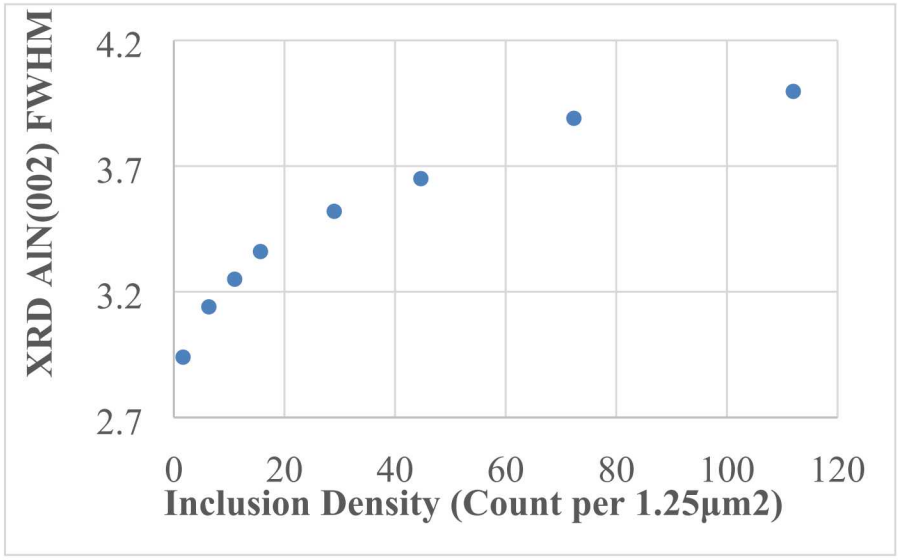

b.

Figure 2. XRD AlN(002) rocking curves for films with varying densities of inclusions (a), and AlN(002) rocking curve FWHM as a function of inclusion density (b).

2.3. GaN grown on PVD AlN on silicon

3-4 µm thick GaN films were grown on 100 nm and 500 nm thick PVD AlN films deposited on Si(100) wafers. The AlN films increased roughness as the film thickness grew; the 100 nm thick AlN film had an Rq of 0.55 nm, while the 500 nm thick AlN film had an Rq of 1.89 nm. AFM images of the AlN film surfaces are shown in Figure 3a, and SEM planar images of the GaN films grown on the AlN films are shown in Figure 3b.

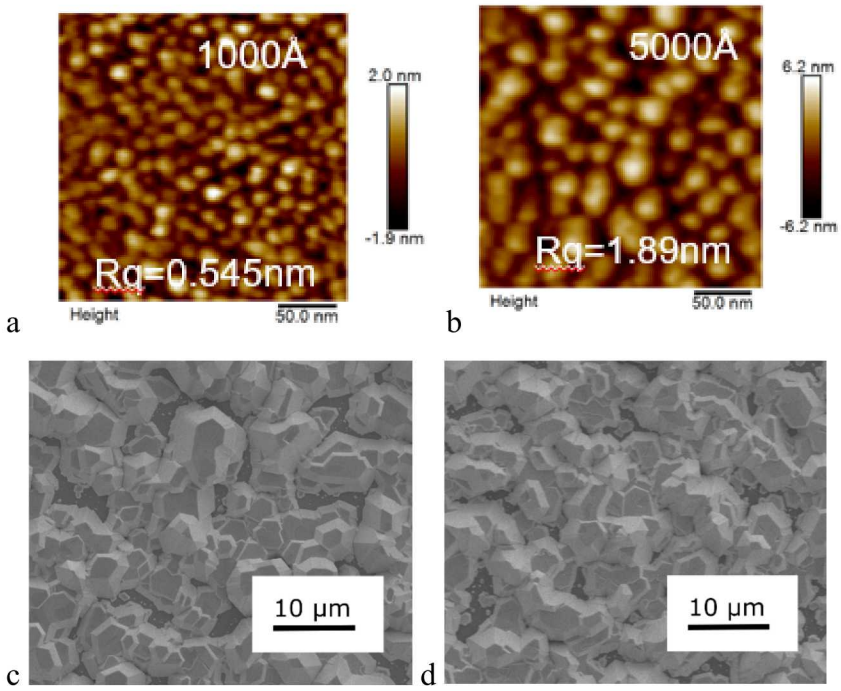

Figure 3. AFM images of 100 nm (a) and 500 nm (b) thick AlN films. Planar SEM images of 3-4 um thick GaN films grown on the 100 nm and 500 nm thick AlN films (c, d respectively)

The GaN films showed some c-axis growth, with a 2.1° GaN(002) rocking curve FWHM for the GaN grown on the 500 nm thick AlN. While promising, the GaN orientation could not be improved unless the AlN film orientation was substantially improved. Due to extenuating circumstances further GaN growths were precluded, so subsequent work focused on improving the AlN film quality.

2.4. AlN Grown on CMOS Substrates

AlN orientation has been demonstrated to have improved orientation by depositing the film on an underlying metal layer such as Pt and Mo [8,9]. However, AlN growth on other commonly available CMOS-compatible substrates, such as TiN and Ta, are not well characterized. TiN and Ta are attractive candidates for use as seeding layers because their melting temperatures are sufficiently high (2930 °C and 3017 °C, respectively) that they can safely be used in the 600-1100 °C MOCVD processes used to deposit GaN, unlike AlCu, which melts at 660 °C.

In order to evaluate AlN growth on TiN and Ta, AlN films of varied thicknesses spanning 100 nm – 1500 nm were reactively sputtered using the SPTS Sigma 200 AlN deposition tool onto metal films deposited on 150 mm Si(100) substrates. The metal films of interest were oriented TiN films (20 nm IMP Ti followed by 50 nm of reactively sputtered TiN, "TiN") and Ta films (100 nm of PVD Ta, "Ta"). AlN films of corresponding thicknesses were also sputtered on well characterized reference substrate materials consisting of oxide films (630 nm thick wet thermal silicon oxide, "oxide") and oriented AlCu films (20 nm of IMP Ti, followed by 50 nm of PVD TiN,

followed by 100 nm AlCu, "AlCu") for comparison. Sufficient time (> 2 days) occurred between the CMOS film depositions and the subsequent AlN depositions such that the AlCu and Ta films had time to form a native oxide, which was not removed prior to the AlN film deposition.

The AlN deposition conditions are given in Table 1. The AlN film stress was measured using an FSM 128NBM film stress measurement tool, and the film thickness of the AlN was measured using a KLA-Tencor UV1080 thin film measurement system. Sheet resistance was measured using a KLA-Tencor Prometrix RS75 four point probe system. XRD measurements were taken using Panalytical X'Pert MPD diffractometer using Cu radiation. SEM measurements were taken using a Zeiss Microscopy Supra 60 SEM and AFM measurements were taken using a Bruker Nan Dimension FastScan 200 atomic force microscope and analyzed using NanoScope Analysis v1.5 software.

Table 1. The deposition conditions for PVD AlN films deposited by the SPTS Sigma 200 tool.

Deposition Parameter	AlN
Ar Flow	100 sccm
N2 Flow	20 sccm
Temperature	350 C
Power (pulsed DC)	5 kW
Pressure	5 mTorr

The roughness and film stress of the CMOS-compatible films are shown in Table 2, and AFM images of the film surfaces are shown in Figure 1.

Table 2. The film properties of the CMOS substrate materials.

	Thermal Oxide	TiN	AlCu	Ta
Rq Roughness (nm)	0.224	0.683	1.24	0.825
Film stress (MPa)		-890	429	-1989

The thermal oxide was the smoothest of the four measured films (0.224 nm), and the AlCu was the roughest (1.24 nm). The TiN and Ta films both had large compressive residual stresses, while the AlCu had a tensile residual stress.

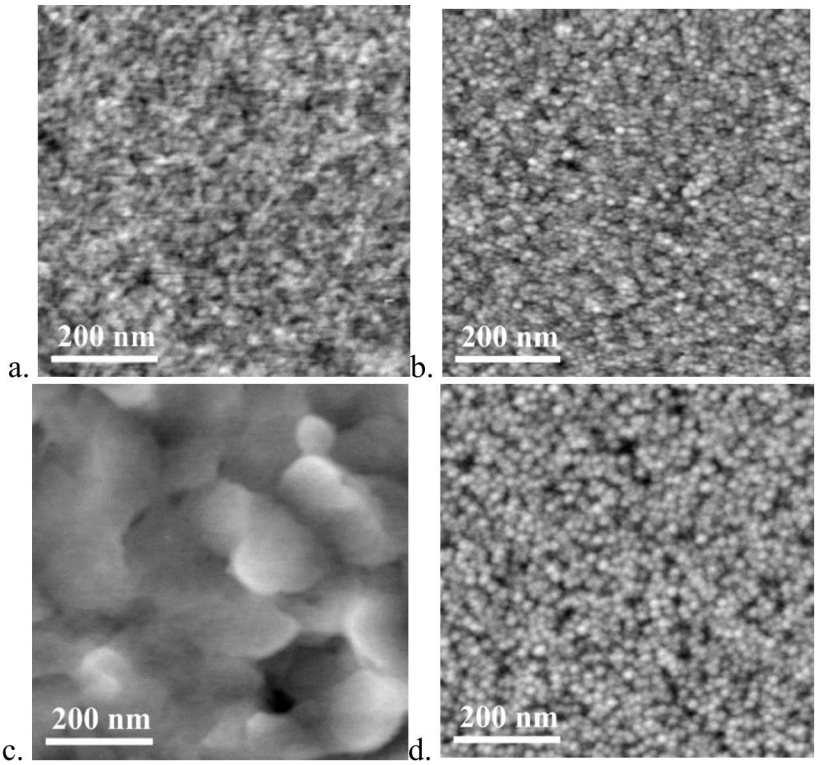

Figure 4. AFM images of the surfaces of the oxide (a), TiN (b), AlCu (c), and Ta (d) films.

The XRD θ-2θ patterns of 750 nm AlN films grown on the CMOS substrates from Figure 1 are shown in Figure 2. The XRD AlN(002) omega rocking curve FWHM values for the AlN films grown on the CMOS substrates as a function of AlN film thickness is shown in Figure 2b. Planar and cross section views of the 750 nm thick films are shown in Figure 3.

All 750 nm thick AlN films displayed c-axis orientation, though the AlN(002) peak was less pronounced for the AlN film grown on TiN. The SEM planar image of the AlN film grown on TiN shows a large number of secondary grain growths similar to those discussed in Section 2.3. This agrees with the rocking curve FWHM data in Figure XRD1b, which shows that AlN films grown on TiN have substantially higher FWHM values than those grown on other substrates. It is unlikely that AlN films grown on TiN would perform well piezoelectrically, given that inclusions have been shown to degrade piezoelectric coupling performance [7].

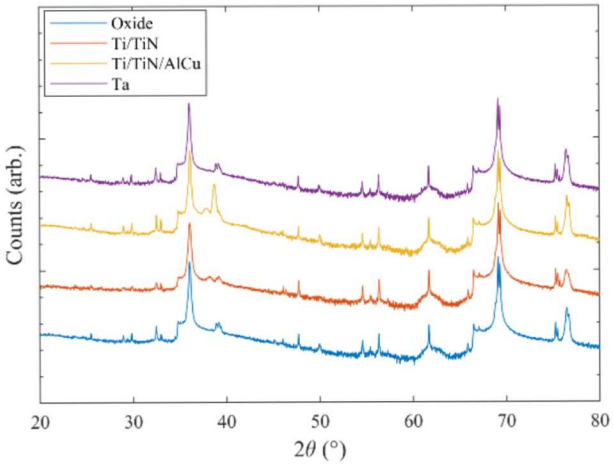
Oxide
Ti/TiN
Ti/TiN/AlCu
Ta
Counts (arb.)
20
30
40
50
60
70
80
2θ (°)

a.

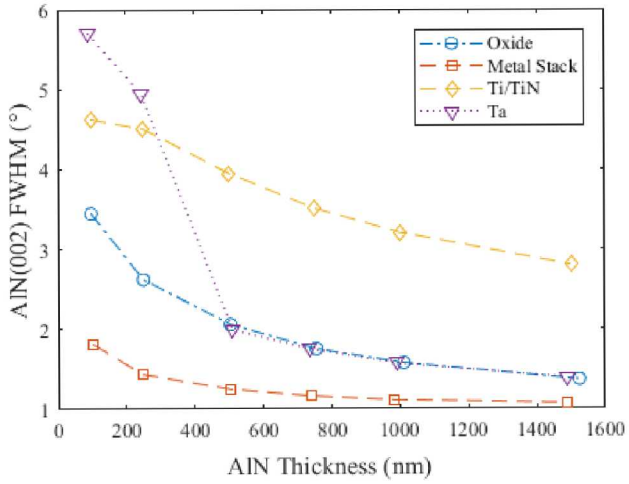
Oxide
Metal Stack
Ti/TiN
Ta
AlN(002) FWHM (°)
1
2
3
4
5
6
0
200
400
600
800
1000
1200
1400
1600
AlN Thickness (nm)

b.

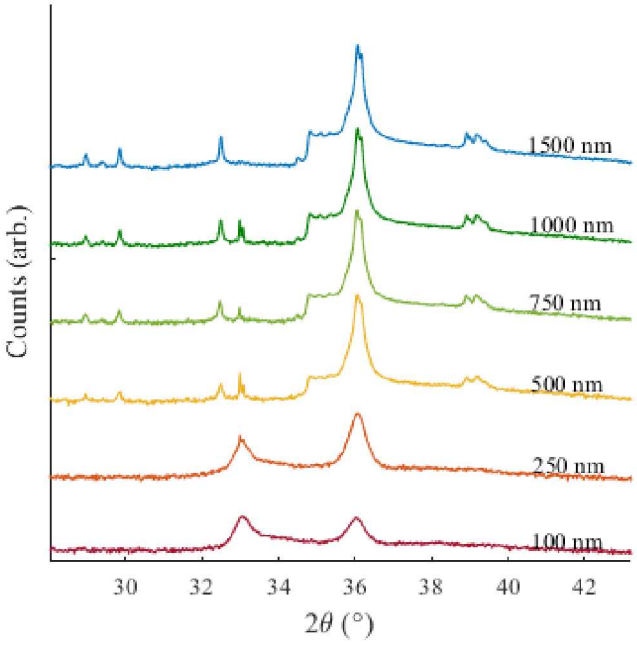

c.

Figure 5. The XRD θ-2θ patterns of 750 nm thick AlN films grown on oxide, TiN, AlCu, and Ta films (a) and the AlN (002) rocking curve FWHM values as a function of AlN film thickness (b). The XRD θ-2θ patterns of AlN films 100 – 1500 nm thick grown on Ta (c).

Despite the film roughness, AlN films grown on AlCu have a substantially lower FWHM than those grown on other substrate materials; this may be due to some degree of epitaxial growth from the oxidized surface of the AlCu. Interestingly, higher surface roughness of the AlCu do not seem to have a negative impact, despite the fact that AlN orientation is improved as the substrate surface roughness is reduced [10].

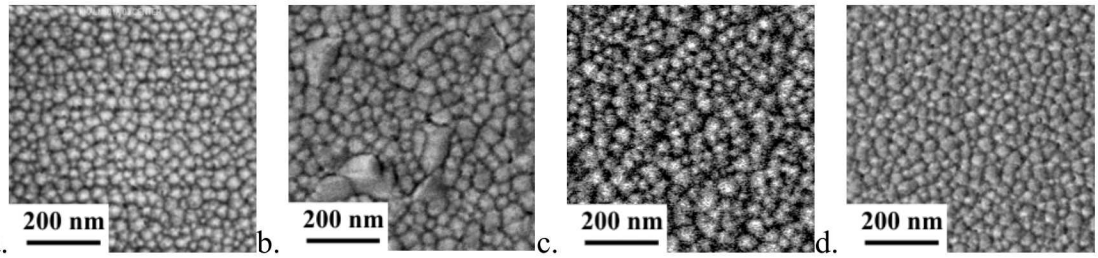

a. b. c. d.

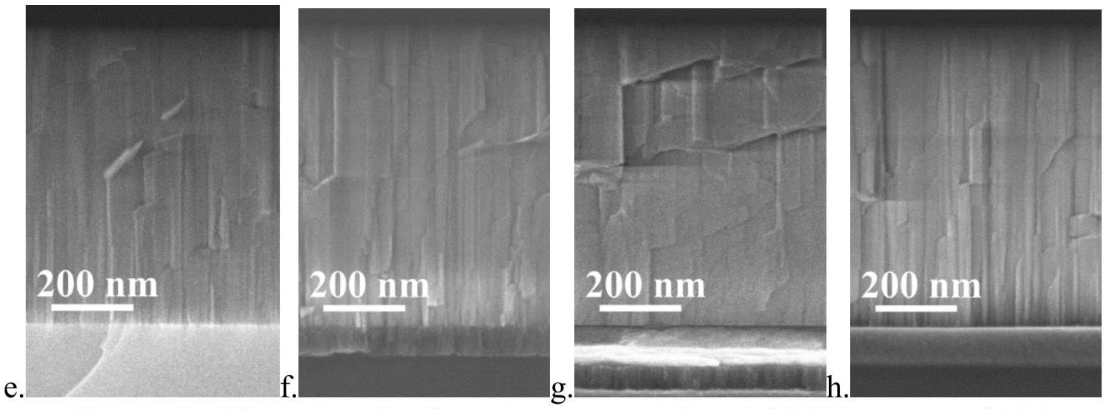

Figure 6. Plan-view (a-d) and cross-sectional SEM images of 750 nm thick AlN films grown on oxide (a,e), TiN (b,f), AlCu (c,g), and Ta (d,h).

AlN grown on Ta initially grows with poor texturing, but the texturing rapidly improves as the films thicken from 250 nm to 500 nm in thickness. For films 500 nm and thicker, the AlN films have good texturing, with rocking curve FWHM values matching those of AlN films grown on oxide.

The thin AlN films (100 nm, 250 nm) grown on β-Ta had poor orientation, but as the film thickened the (002) orientation dominated, as shown in the XRD theta-2theta patterns shown in Figure 2c. This agrees with the XRD AlN(002) full width half maximum (FWHM) data shown in Figure 2b, which shows poor AlN(002) orientation for the thin films, abruptly improving to c-axis orientation as the films thicken past 500 nm. This transition has not been observed in AlN grown on other substrate materials, but was a repeatable phenomenon observed across multiple deposition sets and is worth further investigation.

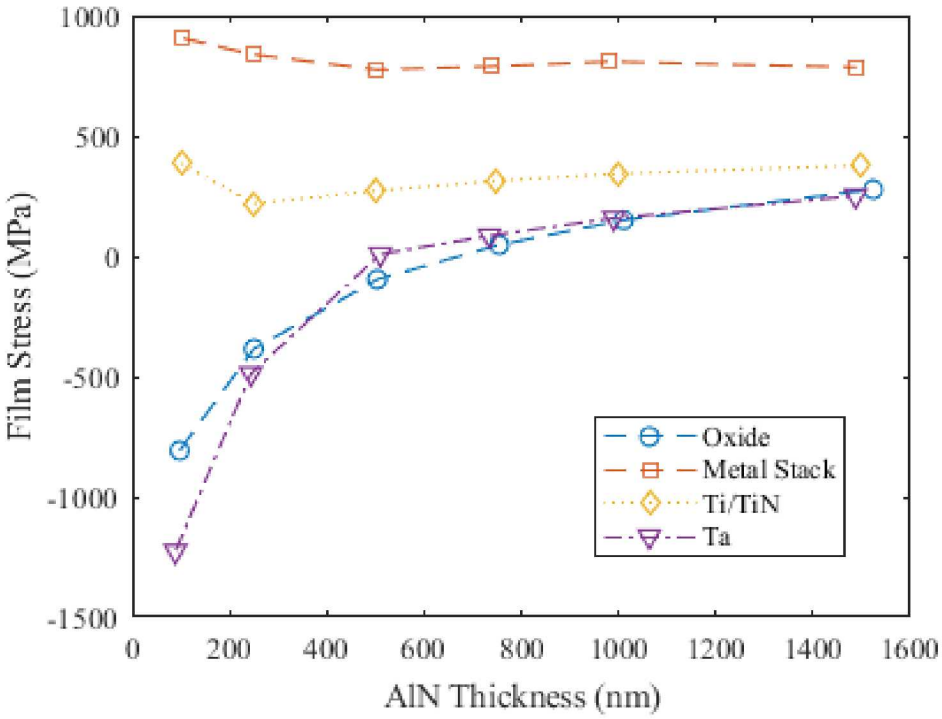

Figure 7. The residual film stress of AlN films grown on CMOS substrates as a function of AlN film thickness.

The AlN film stress on oxide, TiN, AlCu, and Ta as a function of film thickness is shown in Figure 4. The stress evolution of films grown on oxide and Ta are comparable to that observed on Si [1,4]. However, the AlN films grown on TiN and AlCu do not exhibit the same stress gradients. Instead, the film stress consistently tensile for the full AlN thickness range measured. One possible explanation for the large difference in stress behavior between AlN grown on oxide and AlN grown on metal substrates is that the conductivity of the metal blanket films interacts with the substrate and target plasmas to modify the adatom energy conditions, but the Ta film sheet resistance was lower than that of the TiN film, which may indicate that the difference in stress gradient behaviors is due instead to some degree of epitaxial growth occurring between the AlCu, TiN, and AlN films.

In summary, no PVD AlN films grown on CMOS-compatible metals showed AlN orientation sufficient to nucleate high quality GaN films (<1000 arcsec AlN(002) XRD rocking curve FWHM). AlN grown on AlCu had the best orientation, but AlCu is incompatible with the high temperatures used in MOCVD depositions. AlN grown on TiN had poor orientation and is not likely to be of use for optoelectronic or piezoelectric applications. Ta shows promise as a substrate material for use as a bottom electrode for piezoelectric applications, particularly for applications requiring high temperatures, but is not likely to be useful as a nucleation layer to seed AlN NLs for GaN growth.

3. $AL_{0.88}SC_{0.12}N$ CHARACTERIZATION

Recently, the addition of Sc to form a wurtzite $Al_{1-x}Sc_xN$ alloy has been shown to be beneficial for piezoelectric applications because the addition of Sc in to the lattice increases the piezoelectric coefficient d_{33} and piezoelectric coupling coefficient $k_{t,eff}^2$ [11-16]. Improved piezoelectric coupling is of particular interest for filters used for mobile communications, where the critical figure of merit is the $k_{t,eff}^2$-Q product [17], but is of interest for all piezoelectric applications, as an increase in the coupling coefficient means that mechanical energy is more efficiently converted to electrical energy.

In addition to piezoelectric applications, PVD AlN has been demonstrated as a buffer layer to facilitate GaN growth on Si substrates for heterogeneous integration [18-22]. PVD AlN buffer layers are attractive because separating the AlN film growth from the GaN growth eliminates the time-consuming preconditioning process necessary to avoid evaporation of Ga during pregrowth cleaning of the Si wafer [18], and the low temperature AlN deposition process reduces the diffusion of Al into the Si substrate [19]. For this application, Sc doping is of interest because it increases the a-lattice parameter to improve lattice matching to GaN and $Al_xGa_{1-x}N$ [23-26], making $Al_{1-x}Sc_xN$ attractive for use as a buffer layer for optoelectronic applications such as GaN on Si.

3.1. Experimental Method

$Al_{0.88}Sc_{0.12}N$ films were deposited on Si(111) 150 mm wafers using an SPTS Sigma 200 pulsed DC magnetron sputtering system using an $Al_{0.88}Sc_{0.12}$ target (99.9% pure) reactively sputtered in an Ar and N2 environment. Prior to $Al_{0.88}Sc_{0.12}N$ depositions, the Si(111) native oxide was removed using a sputter etch preclean performed in a preclean chamber, and the $Al_{0.88}Sc_{0.12}N$ depositon chamber was pumped to a base pressure of 2×10^{-7} mTorr. Vacuum was not broken between the preclean and deposition steps. Unless otherwise specified, the sputter etch and $Al_{0.88}Sc_{0.12}N$ deposition process parameters are as listed in Table 3.

Table 3. $Al_{0.88}Sc_{0.12}N$ sputter etch and film deposition process conditions

Parameter	Sputter Etch	$Al_{0.88}Sc_{0.12}N$ Deposition
Pedestal Temperature	400C	375C
Chamber Base Pressure	2×10^{-7} Torr	1.4×10^{-7} Torr
Preheat:		
Time	240s	120s
Gas flow	350sccm Ar	--
Process:		
Gas Mixture	Ar	1:4 Ar:N2
Pressure	1.5 mTorr	5.6 mTorr
Power	50W	5kW
Substrate bias	25W	80W

Thickness and refractive index measurements were performed using a Woollam M-2000 ellipsometer. Stress measurements were made using a Toho Technology FLX-2320 stress measurement tool using Stoney's equation

$$T = \frac{Y_s}{6(1-\upsilon_s)} \cdot \frac{{t_s}^2}{t_f} \cdot \left[\frac{1}{R} - \frac{1}{R_0}\right]$$

where Y_s and υ_s are the Young's modulus and Poisson's ratio, t_s is the substrate thickness, t_f is the film thickness, and R_0 and R are the radius of curvature of the substrate before and after deposition, respectively. The Young's modulus and Poisson's ratio used for Si(111) were 168.9GPa and 0.262, respectively [27].

Scanning transmission electron microscopy (STEM) was performed using a FEI Company Titan G2 80-200 operated at 200kV and equipped with an aberration corrector on the probe-forming optics as well as four silicon-drift X-ray detectors. X-ray diffraction (XRD) θ-2θ measurements were made using a Siemens D500 diffractometer and omega rocking curve measurements were made using a Panalytical X'Pert Pro diffractometer in a wide slit configuration; both tools used Cu Kα sources, fixed slits, diffracted-beam monochromators, and scintillation detectors. Tilt-a-whirl data were collected using a Bruker D8 diffractometer with GADDS (Hi-Star area detector) and an Eulerian texture cradle to collect datasets from 2θ, χ, and φ. Surface roughness measurements were made using atomic force microscopy (AFM), using a Digital Instruments D5000 tool and analyzed using NanoScope Analysis v1.5r2. The grain size watershed analyses and height difference correlation calculations were done in MATLAB.

3.2. Thickness Dependence on Si(111) and Si(100) Substrates

Characterization of the thickness dependence of $Al_{0.88}Sc_{0.12}N$ deposited on Si(111) and Si(100) substrates has been discussed in K. Knisely, et al. [28]. Unfortunately, TEM imaging of $Al_{0.88}Sc_{0.12}N$ films grown on Si(111) films showed that the argon sputter etch used to remove the Si(111) native oxide left a layer of argon-rich silicon oxide, preventing direct epitaxial growth of the $Al_{0.88}Sc_{0.12}N$ on the Si(111). A promising direction for future work to would be to develop a method of removing the Si(111) native oxide without leaving an amorphized surface, so that epitaxial growth of $Al_{0.88}Sc_{0.12}N$ on the Si(111) substrate can be achieved.

3.3. Power Dependence on Si(111) Substrates

Approximately 360 nm thick $Al_{0.88}Sc_{0.12}N$ films were deposited as the RF bias and target powers were varied between 60 – 90 W and 3 – 5 kW, respectively. The resulting thicknesses of the films and deposition rates are shown in Figure 8a and b, respectively. While uniform thicknesses were targeted, the films deposited using 3kW target power ended up approximately 20 nm thicker than target and the 5kW films were approximately 20 nm thinner than target. The deposition rate was linear with target power, and the RF bias did not affect deposition rate, which matches the behavior seen in AlN films [4,29].

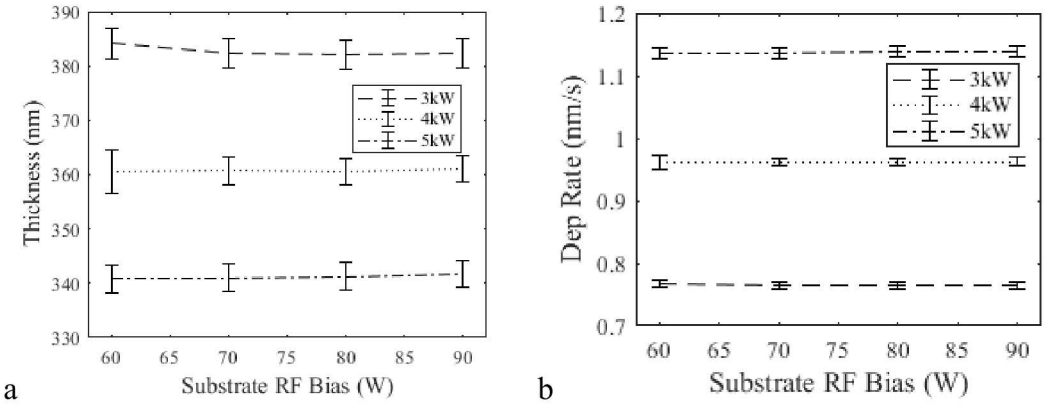

Figure 8. Thickness (a) and deposition rate (b) of $Al_{0.88}Sc_{0.12}N$ films as a function of target power and substrate RF bias power.

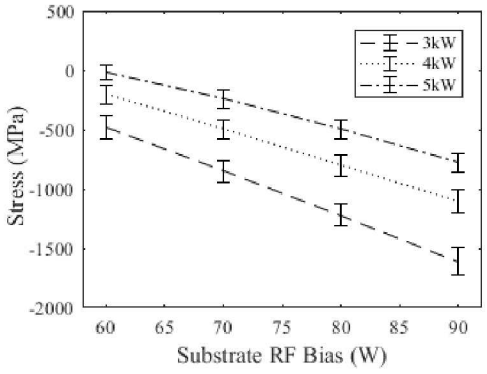

Figure 9. $Al_{0.88}Sc_{0.12}N$ residual film stress as a function of substrate RF bias power and target power.

The residual film stress, as a function of substrate RF bias power and target power, is shown in Figure 9. For a given target power, increasing the RF substrate linearly increases the stress compressively, similar to the bias-stress relationship for AlN described in Knisely et al. [4]. Similarly, the $Al_{0.88}Sc_{0.12}N$ residual film stress also grows more compressive as the target power increases. In both cases the increased energy supplied to the bombarding ions by increasing the power causes a compressive film stress shift due to atomic peening [2]. The 20 nm difference in film thicknesses was calculated to have no more than a 20 MPa effect on the film stress, and therefore does not significantly impact the stress data shown in the figure.

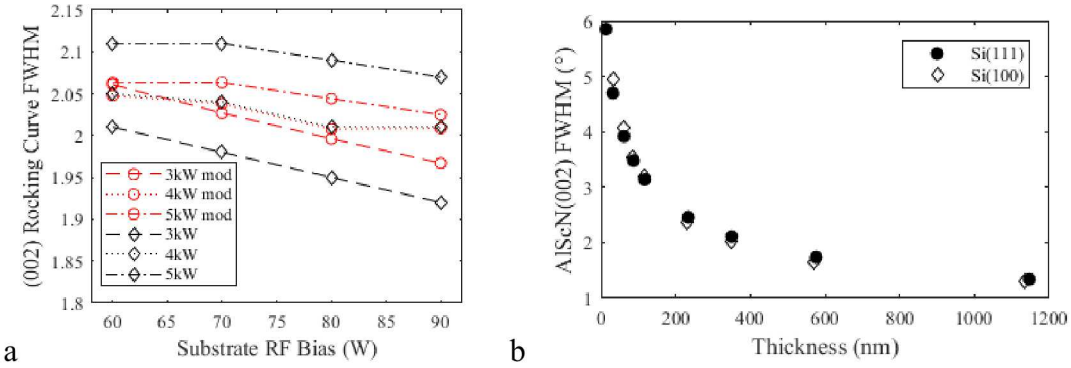

Figure 10. AlScN(002) XRD rocking curve FWHM values as a function of target power and substrate RF bias power (a), and AlScN(002) FWHM values as a function of film thickness (b).

The AlScN(002) XRD rocking curve FWHM values of the films shown in Figure 8 are shown in Figure 10a in black. The film thickness differences of 20 nm are significant enough to impact the FWHM values, as shown in the plot of AlScN(002) FWHM as a function of film thickness in Figure 10b. When the FWHM values of Figure 10a are corrected by compensating for film thickness differences, as shown in red, it can be seen that the target power has minimal impact on the film orientation. Increasing the RF bias substrate bias does have a small net positive impact on film orientation.

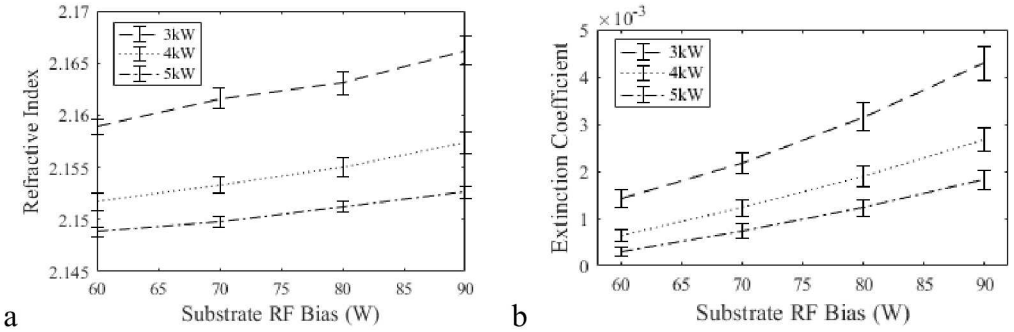

Figure 11. The refractive index (a) and extinction coefficient (b) values as a function of target and substrate RF bias powers.

The refractive index (n) and extinction coefficient (k) values for the $Al_{0.88}Sc_{0.12}N$ films as a function of target power and substrate RF bias are shown in Figure 11a and b, respectively. Increasing the target power lowers the refractive index and extinction coefficient. The variation could be a result of the 20 nm film thickness differences, or it could be that the increased particle flux reaching the wafer surface lowers the n and k values by overwhelming argon incorporation. Increasing the substrate RF bias increases both the n and k values, though the effect is more significant for the k values. This may be likewise a function of increased argon incorporation, as a higher RF bias power will lead to greater amounts of argon incorporation into the film.

Further examination of this effect could be useful for programs that desire AlN and AlScN films with specific optical properties.

3.4. Gas Dependence on Si(111) Substrates

$Al_{0.88}Sc_{0.12}N$ films were deposited using process conditions where the total gas flow (the sum of the argon and nitrogen gas flows) was varied between 100, 125, and 150 sccm, and the gas mixture was varied from 75% nitrogen up to 87% nitrogen. The deposition time was 300s for all films deposited. The film thickness and deposition rates are shown in Figure 12a and b, respectively. Data for the 86% N_2, 100 sccm flow condition was not recorded because the chamber could not sustain a process plasma. Chamber pressure was not held constant as the gas flows were varied. Increasing the total gas flow slightly decreased the deposition rate, and higher nitrogen content also decreased the deposition rate. Both of these are consistent with the fact that increasing the pressure and nitrogen content during deposition reduces the plasma size and quenches the target surface into a more nitridized state. However, the film thickness variations were still relatively small overall, around 10 nm variation, so film property variations due to thickness are less significant than those reported in the Power section above.

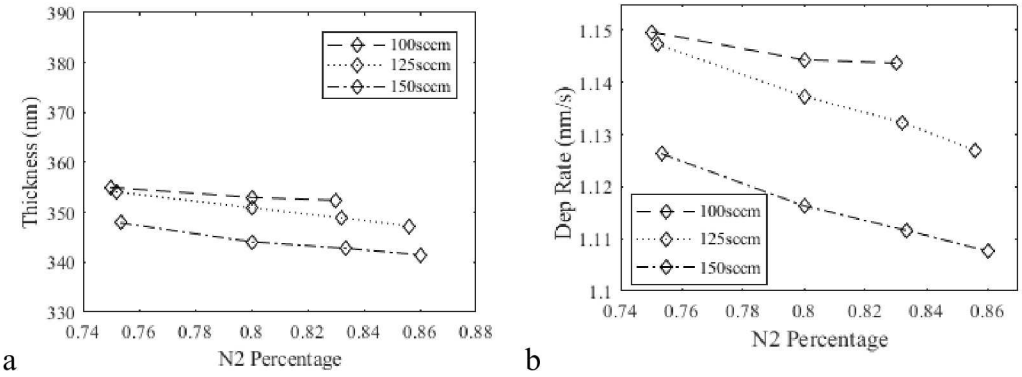

a b

Figure 12. The film thickness (a) and deposition rate (b) values as a function of gas mixture.

The AlScN(002) rocking curve FWHM values and the residual film stress are plotted as a function of gas mixture in Figure 13a and b, respectively. Changes to the mixture flow and nitrogen content did not have any significant impact on the c-axis orientation of the films. Increasing the gas mixture reduces the compressive stress in the films, which is in agreement with reactive sputter theory [2] that states that reducing the mean free path will cause more collisions of particles as they transport to the wafer surface, thus reducing the energy of collisions with the surface. This in turn reduces the atomic peening effect that drives compressive stress in the films. Increasing the nitrogen percentage in the mixture moved the stress slightly more compressive, indicating that the argon plays a larger role in the peening effect than the nitrogen does.

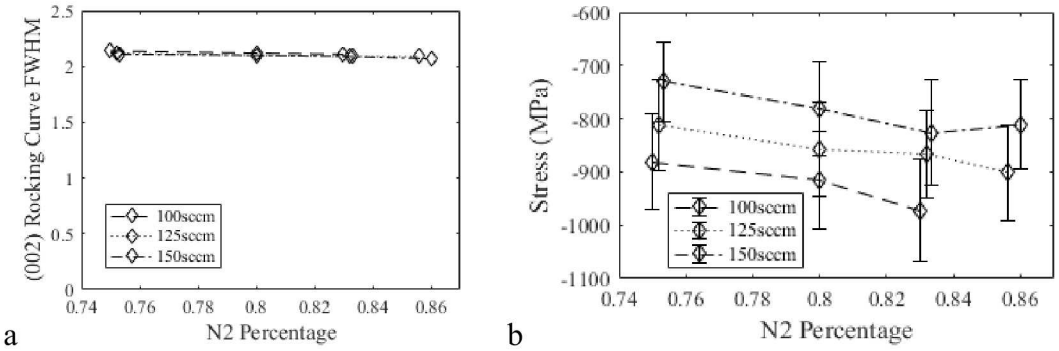

a b

Figure 13. AlScN(002) rocking curve FWHM values (a) and residual film stress (b) as a function of gas mixture.

The n and k values of the $Al_{0.88}Sc_{0.12}N$ films are plotted as a function of gas mixture in Figure. The refractive index was not impacted by the changes to the gas mixture, but increasing the nitrogen percentage did increase the extinction coefficient. This is consistent with the possibility that the extinction coefficient may be driven by the amount of argon incorporation in the films.

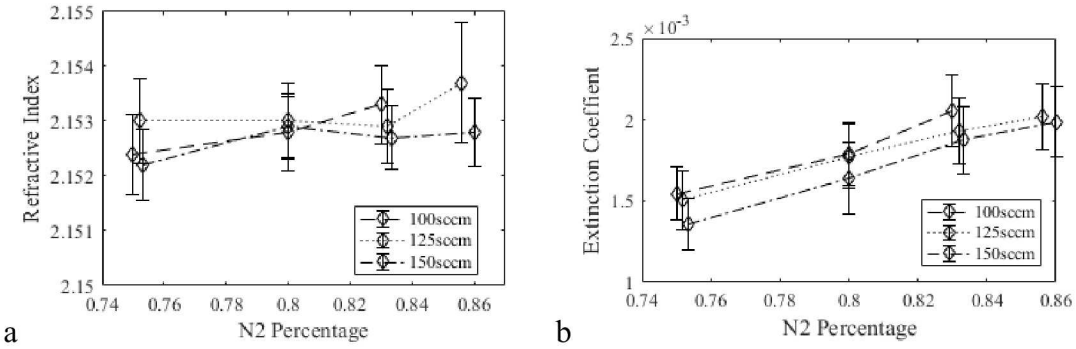

a b

Figure 14. The refractive index (a) and extinction coefficient (b) values as a function of gas mixture.

3.5. $Al_{0.88}Sc_{0.12}N$ Grown on Sapphire

In addition to characterizing $Al_{0.88}Sc_{0.12}N$ grown on Si substrates, $Al_{0.88}Sc_{0.12}N$ was also grown on 50 mm sapphire wafers. In order to deposit the films on the substrates, a pocket wafer was purchased, shown in Figure 15a. This allowed the Sigma 200 deposition tool to deposit $Al_{0.88}Sc_{0.12}N$ or AlN films on four 50 mm wafers at a time, regardless of whether the wafers were transparent or opaque. Initial growths revealed some c-axis orientation, though a large number of triangular inclusions were seen in the films. Further work on this topic is pursued in subsequent work through a separate project.

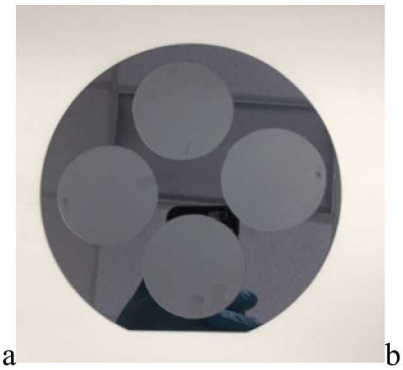

a b

Figure 15. The pocket wafer used to deposit AlScN films on 50 mm wafers (a), and a planar SEM image of the surface of an AlScN film deposited on a 50 mm sapphire substrate.

4. CONCLUSIONS

AlN and $Al_{0.88}Sc_{0.12}N$ films were developed and characterized for use as nucleation layers to grown GaN on Si, metal, and sapphire substrates. A model for predicting and controlling the AlN intrinsic film stress was developed, in order to tailor AlN film stress to minimize cracking in subsequently deposited GaN films. Additionally, AlN films were grown on TiN, AlCu, oxide, and Ta, in order to evaluate whether a metal interlayer deposited between the AlN and the Si substrate would improve AlN orientation. AlN films grown on AlCu had excellent properties, but AlCu is not compatible with the high temperatures used in MOCVD GaN growth. AlN films grown on TiN were of poor quality, and AlN films grown on oxide and Ta showed similar film orientation to those grown on Si. AlN grown on Ta may be of further interest for high temperature piezoelectric applications. GaN films were grown on sputtered AlN films and showed some c-axis orientation, but the GaN orientation was limited by the quality of the orientation of the AlN films. AlScN (12% Sc) films grown on Si(111) and Si(100) were characterized for film properties such as texture, roughness, grain size, and stress for a variety of $Al_{0.88}Sc_{0.12}N$ film thicknesses, target and substrate bias powers, and gas mixtures. $Al_{0.88}Sc_{0.12}N$ film orientation improves and the films coarsen as the film thickens. Doping AlN with Sc was found to expand the a-axis and c-axis lattice parameters, resulting in an improved lattice match to GaN. Finally, a process was developed to deposit $Al_{0.88}Sc_{0.12}N$ films on sapphire substrates to evaluate whether epitaxial growth of $Al_{0.88}Sc_{0.12}N$ on sapphire improved the $Al_{0.88}Sc_{0.12}N$ orientation. The films showed some c-axis orientation, but large secondary grain growths were also observed. A high temperature anneal may improve the film texture, and further work is being done to evaluate $Al_{0.88}Sc_{0.12}N$ for use as a nucleation layer for AlGaN growth on sapphire.

REFERENCES

1. Martin F, Muralt P, Dubois M A and Pezous A 2004 Thickness dependence of the properties of highly c-axis textured AlN thin films *J. Va. Sci. Technol A* **22** 361-365

2. Thompsonn C V 2000 Structure evolution during processing of polycrystalline films Annu. Rev. Mater. Sci **30** 159-190

3. McAlesse C, Kappers M J, Rayment F D G, Cherns P, and Humphreys C J 2004 Strain effects of AlN interlayers for MOVPE growth of crack-free AlGaN and AlN/GaN multilayers on GaN *J. Cryst. Growth* **272** 475-480

4. Knisely K, Hunt B, Troelsen B, Douglas E, Griffin B A, and Stevens J E 2018 Method for controlling stress gradients in PVD aluminum nitride *J. Micromech. Microeng.* **28** 115009

5. Knisely K, Griffin B, Timon R, Young T, Monochie M, Dallo H, and Olewine M 2017 Effect of Oxygen Contamination on PVD AlN Growth 2017 *International Conference on Metallurgical Coatings and Thin Films,* oral presentation

6. Fichtner S, Wolff N, Krishnamurthy G, Petraru A, Bohse S, Lofink F, Chemnitz S, Kohlsedt H, Keinle L, and Wagner B 2017 Identifying and overcoming the interface originating c-axis instability in highly Sc enhanced AlN for piezoelectric micro-electromechanical systems *J. Appl. Phys.* **122** 035301

7. Clement M, Olivares J, Iborra E, Gonzalez-Castilla S, Rimmer N, and Rastogi A 2009 Aln films sputtered on iridium electrodes for bulk acoustic wave resonators *Thin Solid Films* **517** 4673-4678

8. Martin F, Muralt P, and Dubois M A 2006 Process optimization for the sputter deposition of molybdenum thin films as electrode for AlN thin films *J. Vac. Sci. Technol. A* **24** 946-952

9. Dubois M A, Muralt P 1999 Properties of aluminum nitride thin films for piezoelectric transducers and microwave filter applications *Appl. Phys. Lett.* **74** 3032-3034

10. Artieda A, Barbieri M, Sandu C S, and Muralt P 2009 Effect of substrate roughness on c-oriented AlN thin films *J. Appl. Phys.* **105** 024504

11. Akiyama M, Kamohara T, Kano K, Teshigahara A, Takeuchi Y, Kawahara N, 2009 Enhancement of piezoelectric response in scandium aluminum nitride alloy thin films prepared by dual reactive cosputtering, *Adv. Mater.* **21** 593-596

12. M. Akiyama, K. Kano, A. Teshigahara, Influence of growth temperature and scandium concentration on piezoelectric response of scandium aluminum nitride alloy thin films, Appl. Phys. Lett. 95 (2009) 162107, doi:10.1063/1.3251072

13. F. Tasnádi, B. Alling, C. Höglund, G. Wingqvist, J. Birch, L. Hultman, I.A. Abrikosov, Origin of the anomalous piezoelectric response in wurtzite Sc¬xAl1-xN alloys, Phys. Rev. Let. 104 (2010) 137601, doi:10.1103/PhysRevLett.104.137601

14. M. Moriera, J. Bjurström, I. Katardjev, V. Yantchev, Aluminum scandium nitride thin-film bulk acoustic resonators for wide band applications, Vacuum 86 (2011) 23-26, doi:10.1016/j.vacuum.2011.03.026

15. W. Wang, P.M. Mayrhofer, X. He, M. Gillinger, Z. Ye, Z. Wang, A. Bittner, U. Schmid, J.K. Luo, High performance AlScN thin film based surface acoustic wave devices with large electromechanical coupling coefficient, Appl. Phys Lett. 105 (2014) 133502, doi:10.1063/1.4896853

16. M.D. Henry, R. Timon, T.R. Young, C. Nordquist, B. Griffin, AlN and ScAlN Contour Mode Resonators for RF Filters, ECS Trans. 77 (2017) 23-32, doi:10.1149/07706.0023ecst

17. G. Piazza, V. Felmetsger, P. Muralt, R.H. Olsson, R. Ruby, Piezoelectric aluminum nitride thin films for microelectromechanical systems, MRS Bulletin 37 (2012) 1051-1061, doi:10.1116/1.1649343

18. H. Wang, H. Sodabanlu, Y. Diago, T. Seino, T. Nakagawa, and M. Sugiyama, Initial growth control of GaN on Si with physical-vapor-deposition-AlN seed layer for high-quality GaN templates, Appl. Phys. Exp. 9 (2016) 055503, doi:10.7567/APEX.9.055503

19. T. Yamada, T. Tanikawa, Y. Honda, M. Yamaguchi, and H. Amano, Growth of GaN on Si(111) substrates via a reactive sputter-deposited AlN intermediate layer, Jap. J. Appl. Phys. 52 (2013) 08JB16, doi:10.7567/JJAP.52.08JB16

20. J. H. Yang, S. M. Kang, D.V. Dinh, D.H. Yoon, Influence of AlN buffer layer thickness and deposition methods on GaN epitaxial growth, Thin Solid Films 517 (2009) 5057-5060, doi:10.7567/JJAP.54.071001

21. J. C. Gagnon, J.M. Leathersich, F. Shahedipour-Sandvik, J.M. Redwing, The influence of buffer layer coalescence on stress evolution in GaN grown on ion implanted AlN/Si(111) substrates, J. Cryst. Growth, 393 (2014) 98-102, doi:10.1016/j.jcrysgro.2013.08.031

22. M. Tungare, X. Weng, J.M. Leathersich, P. Suvarna, J.M. Redwing, F. Shahedipour-Sandvik, Modification of dislocation behavior in GaN overgrown on engineered AlN film-on-bulk Si substrate, J. Appl. Phys. 113 (2013) 163108, doi:10.1063/1.4798598

23. M. Akiyama, K. Kano, A. Teshigahara, Influence of growth temperature and scandium concentration on piezoelectric response of scandium aluminum nitride alloy thin films, Appl. Phys. Lett. 95 (2009) 162107, doi:10.1063/1.3251072

24. C. Höglund, J. Birch, B. Alling, J. Bareño, Z. Czigány, P.O.A. Persson, G. Wingqvist, A. Zukauskaite, L. Hultman, Wurtzite structure of Sc1-xAlxN solid solution films grown by reactive magnetron sputter epitaxy: structural characterization and first-principles calculations, J. Appl. Phys. 107 (2010) 123515, doi:10.1063/1.3448235

25. W. Liauh, S. Wu, J-L. Huang, D-F. Lii, Z. Lin, W-K. Yeh, Microstructure and piezoelectric properties of reactively sputtered highly c-axis ScxAl¬¬1-xN thin films on diamond-like carbon/Si substrate, Surf. Coat. Technol. 308 (2016) 101-107, doi:10.1016/j.surfcoat.2016.06.097

26. M. A. Moram, S. Zhang, ScGaN and ScAlN: emerging nitride materials, J. Mater. Chem. A 2 (2014) 6042, doi:10.1039/C3TA14189F

27. J. Kim, D.D. Cho, R.S. Muller, Why is (111) silicon a better mechanical material for MEMS? Transducers 01 Eurosensors XV (2001) 662-665, doi:10.1007/978-3-642-59497-7_157

28. Knisely K, Douglas E, Mudrick M, Rodriguez M, Kotula P 2018 Thickness dependence of $Al_{0.88}Sc_{0/12}N$ thin films grown on silicon, submitted to Thin Solid Films

29. Knisely K and Grosh K 2014 Effect of AC target power on AlN film quality *J. Vac. Sci. Technol. A* **32** 051504

DISTRIBUTION

1	MS0646	Katherine Knisely	2631 (electronic copy)
1	MS1086	Mary Crawford	1800 (electronic copy)
1	MS0899	Technical Library	9536 (electronic copy)
1	MS0359	D. Chavez, LDRD Office	1911

Sandia National Laboratories